

Comparative study of wind turbine emulator control using an asynchronous motor: IRFOC and DTC

Hana Zekraoui¹, Taoufik Ouchbel¹, Mohamed Larbi El Hafyani²

¹Laboratory of Electrical Engineering and Maintenance, University Mohammed 1, High School of Technology Oujda, Oujda, Morocco

²University Mohammed 1, National School of Applied Sciences Oujda, Oujda, Morocco

Article Info

Article history:

Received Feb 5, 2024

Revised Jun 6, 2024

Accepted Jun 25, 2024

Keywords:

Direct torque control

Indirect vector control

Renewable energy

Wind emulator

Wind turbine

ABSTRACT

This work is an overview of one of the renewable energy sources, wind power. The high cost of testing wind turbines and analyzing their characteristics in research laboratories prompted us to create the Wind Emulator. In this article, we will proceed with the development of an emulator of a wind turbine conversion chain based on an asynchronous machine. This emulator would be capable of faithfully reproducing the dynamic characteristics of a real wind turbine and of integrating them optimally into a real electrical system so as to be able to study its operation at laboratory level, so our objective is to have an emulator that will provide the characteristics (speed-torque-current) in real time and with realistic conditions. Our development approach is based on the use of two classical control strategies under the MATLAB/Simulink closed-loop environment: direct torque control (DTC) and indirect rotor flux vector control (IRFOC) in dynamic and static regimes. The simulation results presented and discussed in this work enable us to determine the operating limits of our proposed wind emulator, in order to validate the most suitable emulator model. Ultimately, this model will be integrated into an intelligent computing board such as the DSP1104.

This is an open access article under the [CC BY-SA](https://creativecommons.org/licenses/by-sa/4.0/) license.



Corresponding Author:

Hana Zekraoui

Laboratory of Electrical Engineering and Maintenance, University Mohamed 1

High School of Technology Oujda

BP: 473, 60000, Oujda, Morocco

Email: hanae.zekraoui@ump.ac.ma

1. INTRODUCTION

The development and use of green energies have seen strong growth in recent years. Among these energy sources, wind turbines offer considerable potential. It is not intended to replace existing energies, but to compensate for increasingly rapid demand damping, and also as a rigorous solution for reducing CO₂ emissions. Several recent studies [1]-[7] have indicated that electrical engineering researchers are currently carrying out a variety of activities to improve wind power quality. These research efforts focus on both large wind turbines connected to the power grid and small stand-alone wind turbines. The researches [8]-[10], the authors highlighted the fact that, thanks to this work, the latest generations of wind turbines operate at variable speed in order to extract maximum electrical power as a function of wind speed. The development of power electronics control techniques has made it possible to introduce intelligent controls.

Thus, the field of AC machine control is always evolving, this is due to the requirements of the specifications of industrial operations. The researches [5]-[7], the authors chose the asynchronous machine, due to its low cost and robustness, which has currently become one of the most widely used machines for variable-speed applications. Due to its structure, the asynchronous machine has a significant coupling of

these quantities relative to the DC machine. In fact, because the machine is powered by a single armature, the same current creates both flux and torque, so that variations in torque cause variations in flux, making the control model more complex. The joint development of power electronics and digital electronics has contributed to the development of more advanced control algorithms improving the static and dynamic performance of this machine, and thus ensuring the decoupling of flux and torque. The main problem encountered in wind power applications in laboratories is to produce a wind emulator capable of meeting the requirements of users and researchers in the field of wind energy. The main objective of this work is to carry out a comparative study between indirect rotor flux vector control (IRFOC) and direct torque control (DTC) of the asynchronous machine, in order to produce a wind emulator capable of reproducing the dynamic characteristics of a real wind turbine and integrating them optimally into a real electrical system [11]-[13]. This document is organized as follows. In section 2, you will find a detailed illustration of the description and modeling of the proposed wind emulator. The methodology used to implement the IRFOC and DTC techniques will be presented in section 3, entitled "Method". The results of both methods will then be presented in section 4. Conclusions are presented in section 5.

2. DESCRIPTION AND MODELING OF THE PROPOSED WIND TURBINE EMULATOR

2.1. Description of the wind turbine emulator (WTE)

Before deploying a wind power system, it is necessary to evaluate its behavior in static and dynamic regimes, and to investigate the design of the power electronics and associated controllers in a laboratory environment, in order to avoid problems during installation. To this end, a WTE is an important piece of equipment used to simulate the static, dynamic and non-linear characteristics of a real wind turbine, and is therefore crucial for the development of wind energy conversion systems, which rely neither on natural wind resources nor on a real wind turbine [14]-[21].

In the literature, several wind emulators have been designed and built. In general, the emulator WTE is built by coupling the generator shaft to a motor called the main motor. Three main types of motor have been considered in various works. The first is a DC motor [22]; the second is a permanent magnet synchronous motor (PMSG) [23], [24], and the third uses an asynchronous motor (ASM) [25]. It is possible to generate the same static and dynamic characteristics as a real wind turbine by controlling the main motor.

In our work, the designed wind emulator is schematically shown in Figure 1 and consists of two parts; the first part consists of a DC power source, a voltage inverter to feed the ASM called main motor, which is mechanically coupled with the generator shaft, and which is in turn coupled to a stand-alone load or coupled to the power grid via a transformer. For the asynchronous generator, self-excitation (reactive energy) is provided by capacitor banks mounted across the machine's stator windings or via the electrical grid. The second part of the emulator represents the effect of the quantities involved in the turbine, which generates the aerodynamic torque that is applied to the gearbox. The turbine input is the actual wind speed. The gearbox model transforms mechanical speed and aerodynamic torque into turbine speed and gearbox torque respectively. The shaft model describes the dynamics of the mechanical speed, so it has two inputs: the gearbox torque and the electromagnetic torque supplied by the generator. The control system proposed in the present work has enabled us to control aerodynamic torque and mechanical rotational speed by generating a signal to control the inverter based on various conventional control techniques, in particular IRFOC and DTC.

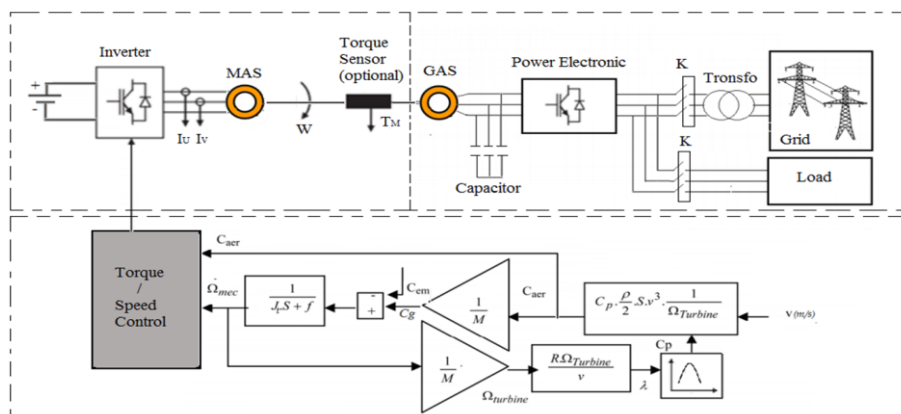


Figure 1. Wind turbine emulator

2.2. Modeling of the WTE

2.2.1. Turbine section model

The total kinetic power available to a wind turbine is given by (1).

$$P_v = \frac{\rho \cdot \pi \cdot R^2 \cdot V^3}{2} \quad (1)$$

With: ρ : air density (1.25 kg/m³); R: blade length; V: wind speed (m/s)

The aerodynamic power on the shaft is given by (2).

$$P_{aer} = C_p(\lambda) \cdot \frac{\rho \cdot \pi \cdot R^2 \cdot V^3}{2} \quad (2)$$

The power coefficient C_p , which represents the aerodynamic performance of a wind turbine, may not exceed 0.59. This performance is expressed by (3).

$$C_p(\lambda) = \frac{G \cdot \lambda \cdot (\lambda_0 - \lambda)}{a^2 + (\lambda_0 - \lambda)^2} \quad (3)$$

λ : the speed ratio can be defined as the ratio between the linear speed of the turbine blades and the wind speed.

$$\lambda = \frac{\Omega_{\text{turbine}} \cdot R}{V} \quad (4)$$

With Ω_{turbine} : turbine speed.

The aerodynamic torque can be determined directly from the turbine speed using the (5).

$$C_{aer} = \frac{P_{aer}}{\Omega_{\text{turbine}}} = C_p(\lambda) \cdot \frac{\rho \cdot S \cdot V^3}{2} \cdot \frac{1}{\Omega_{\text{turbine}}} \quad (5)$$

The gearbox is used to adapt the slow rotation speed of the turbine to the speed of the generator. This adaptation is mathematically modeled by the (6)-(8).

$$C_g = \frac{C_{aer}}{G} \quad (6)$$

$$\Omega_{\text{turbine}} = \frac{\Omega_{\text{mec}}}{G} \quad (7)$$

$$J = \frac{J_{\text{turbine}}}{G^2} + J_g \quad (8)$$

With: G: Gearbox gain; J: Total inertia; J_g : Generator inertia.

The fundamental equation of dynamics allows us to determine the evolution of mechanical speed from the total mechanical torque C_{mec} applied to the rotor:

$$J \frac{d\Omega_{\text{mec}}}{dt} = C_{\text{mec}} = C_g - C_{em} - C_f \Omega_{\text{mec}} \quad (9)$$

With: C_{em} : electromagnetic torque; C_f : coefficient of viscous friction

2.2.2. Modeling of the ASM

The asynchronous machine model used in this study is the classical model in the Park's reference frame. This model is described as follows:

$$\begin{cases} V_{ds} = R_s I_{ds} + \frac{d\phi_{ds}}{dt} - \omega_s \phi_{qs} \\ V_{qs} = R_s I_{qs} + \frac{d\phi_{qs}}{dt} + \omega_s \phi_{ds} \\ V_{dr} = R_r I_{dr} + \frac{d\phi_{dr}}{dt} - (\omega_s - \omega_r) \phi_{qr} \\ V_{qr} = R_r I_{qr} + \frac{d\phi_{qr}}{dt} + (\omega_s - \omega_r) \phi_{dr} \end{cases} \quad (10)$$

$$\begin{cases} \varphi_{ds} = L_s I_{ds} + M I_{dr} \\ \varphi_{qs} = L_s I_{qs} + M I_{qr} \\ \varphi_{dr} = L_r I_{dr} + M I_{ds} \\ \varphi_{qr} = L_r I_{qr} + M I_{qs} \end{cases} \quad (11)$$

With: V_{ds} , V_{qs} , V_{dr} , and V_{qr} ; I_{ds} , I_{qs} , I_{dr} , and I_{qr} are the direct and quadrature stator and rotor voltages and currents, respectively, in the two-phase system. φ_{ds} , φ_{qs} , φ_{dr} , and φ_{qr} : direct and quadrature stator and rotor fluxes of the two-phase system. R_s , R_r , L_s , L_r are the stator and rotor resistances and inductances respectively, and M is the magnetizing inductance.

The electromagnetic torque is given by (12).

$$C_{em} = p \frac{M}{L_r} (I_{sq} \varphi_{rd} - I_{sd} \varphi_{rq}) \quad (12)$$

2.3. IRFOC

The fundamental principle of vector control is to control an asynchronous machine in a similar way to an independently excited DC machine. The aim is to create a natural decoupling between the magnitude controlling the magnetic flux (rotor flux) and that controlling the stator current. The principle of flux orientation control consists in placing the rotating (d-q) reference frame so that the d axis coincides with the rotor flux vector axis see in Figure 2. Thus: $\varphi_{dr} = \varphi_r$ and $\varphi_{qr} = 0$.

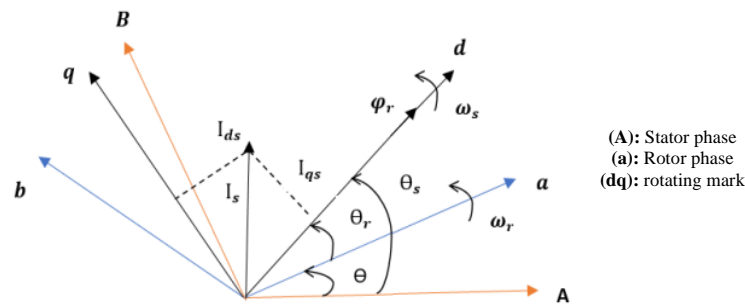


Figure 2. Rotor flux oriented on the d-axis

By orienting the magnetic flux in this way, the electromagnetic torque is reduced to:

$$C_{em} = p \frac{M}{L_r} (I_{sq} \varphi_{rd}) \quad (13)$$

P is a constant, it appears in the torque expression and depends on the nature of the park transformation (abc-dq) chosen (P can take the value $2/3$ for an amplitude-preserving transformation or the value 1 for a power-preserving transformation). According to equation 13, the flux-oriented control strategy aims to independently control flux and stator current in order to regulate the electromagnetic torque developed by the asynchronous machine. This approach establishes a natural decoupling between these two quantities, similar to control in the case of a DC machine. Returning to the equations; by imposing $\varphi_{qr} = 0$, the equations of the machine in a reference frame linked to the rotating field become:

$$\varphi_r = \varphi_{dr} \quad (14)$$

$$\begin{cases} V_{ds} = R_s I_{ds} + \sigma L_s \frac{dI_{ds}}{dt} + \frac{M}{L_r} \frac{d\varphi}{dt} - \omega_s \sigma L_s I_{qs} \\ V_{qs} = R_s I_{qs} + \sigma L_s \frac{dI_{qs}}{dt} + \omega_s \frac{M}{L_r} \varphi_r + \omega_s \sigma L_s I_{ds} \end{cases} \quad (15)$$

$$C_e = p \frac{M}{L_r} \varphi_r I_{qs} \quad (16)$$

$$\omega_r = \frac{M}{\tau_r \varphi_r} I_{qs} \quad (17)$$

$$\tau_r \frac{d\varphi_r}{dt} + \varphi_r = MI_{ds} \quad (18)$$

In indirect control, the park angle θ_s is determined using the stator pulsation, itself reconstructed using the machine speed and rotor pulsation ω_r . In this type of control, the angle θ_s used for the direct and inverse transformations is calculated using the (19).

$$\theta_s = \int \left(p\Omega + \frac{I_{qs}^*}{\tau_r I_{ds}^*} \right) dt \quad \text{Or } I_{ds}^* = \frac{\varphi_r^*}{M} \quad (19)$$

2.4. DTC

Direct torque control for an asynchronous machine is based on the "direct" determination of the control sequence applied to the switches of a voltage inverter. This choice is generally motivated by the use of hysteresis controllers, whose function is to control the state of the system, in particular the amplitude of stator flux and electromagnetic torque. This approach falls into the category of amplitude control, as opposed to more traditional control methods based on pulse-width modulation (PWM) to adjust the mean value of the voltage vector. Originally, DTC controls were largely based on physical common sense and a relatively empirical approach to the variation of states (torque, flux) over a very short time interval.

Dynamic torque control of the asynchronous machine can be illustrated by the vector model of the asynchronous machine. In the reference frame (d, q) linked to the stator, we can write:

$$\begin{cases} V_s = R_s I_s + \frac{d\phi_{ds}}{dt} \\ V_r = R_r I_r + \frac{d\phi_r}{dt} - j\omega_r \cdot \phi_r \end{cases} \quad (20)$$

The vector of the voltage V_s delivered by a three-phase voltage inverter is represented in theory by three Boolean control quantities S_j ($j = a, b, c$) such that:

$$\begin{cases} \{S_j (j = a, b, c) = 1 : \text{High switch closed and low switch open} \\ \{S_j (j = a, b, c) = 0 : \text{High switch open and low switch closed} \end{cases}$$

The voltage vector V_s can be written as (21):

$$V_s = 3/2 \cdot U_0 (S_a + S_b \cdot e^{j\frac{2\pi}{3}} + S_c \cdot e^{j\frac{4\pi}{3}}) \quad (21)$$

Combinations of the three quantities (S_a, S_b, S_c) generate of 8 V_s vector positions, 2 of which correspond to the zero vector: (S_a, S_b, S_c) = (000) or (S_a, S_b, S_c) = (111).

From (20), we can write:

$$\phi_s = \int (V_s - R_s i_s) dt; \quad \phi_s = \phi_{s0} + V_s t - R_s \int i_s dt \quad (22)$$

Assuming that R_s remains constant and the term ($R_s i_s$) is negligible compared to the voltage V_s . In a time interval T_e , the end of the vector ϕ_s moves along a line whose direction is given by V_s see in Figure 3. By selecting a correct sequence of V_s vectors over successive time intervals of duration T_e , the end of the ϕ_s vector can be made to follow the desired trajectory. To achieve this objective, the controller used for DTC is a two-level hysteresis controller. With this type of controller, it is easy to keep the end of the flux vector ϕ_s within a nearly circular ring.

In order to rapidly increase angle γ and therefore torque, it is essential to advance the stator flux vector in the direction of rotation considered positive. In Figure 3, we can see that this can be achieved by applying a voltage vector with a strong forward quadrature component with respect to the flux vector. Conversely, an algebraic reduction in motor torque can be achieved rapidly by applying a voltage vector with a strong quadrature lag component. Electromagnetic torque variations can be controlled solely from the flux vector ϕ_s rotation speed. The table in Figure 4 shows the evolution of flux and torque quantities for each of the four vectors $V_{i+1}, V_{i+2}, V_{i-1}, V_{i-2}$ that can be applied in the Z_i zone. The voltage vectors to be applied depend on the zone where the flux vector is located. The parameters $z_1, z_2, z_3, z_4, z_5, z_6$ see in Figure 4 represent the six possible operating zones.

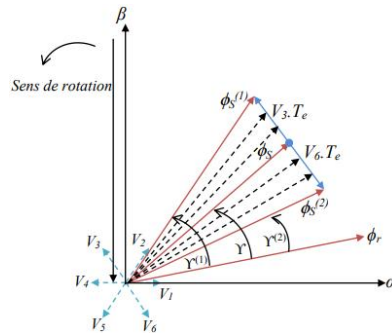


Figure 3. Evolution of the end of the vector ϕ_s

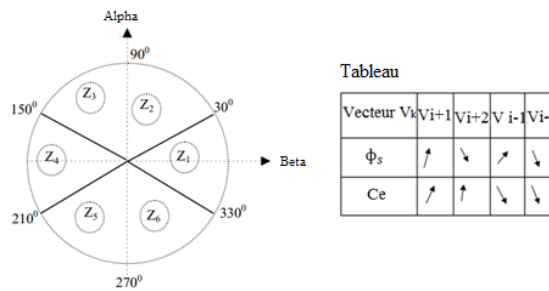


Figure 4. Evolution of flux and torque quantities as a function of the vector V_k applied in the zone Z_i $K = (i-1, i-2, i+1, i+2)$

3. METHOD

3.1. Wind emulator design integrating IRFOC control

The designed wind emulator shown in Figure 5 consists of an asynchronous motor mechanically coupled to the generator. The control strategy is based on IRFOC, which is developed and simulated in the MATLAB/Simulink environment, allowing for precise reproduction of the dynamic characteristics found in a real wind turbine. In the turbine model, we have taken into account the power coefficient in (3) to produce precise dynamic characteristics similar to a real wind turbine. This allows us to adapt the appropriate power coefficient to the type of generator coupled. The input parameters for the wind turbine include the wind speed profile and the rotational speed on the drive motor shaft. The IRFOC control system enabled us to control speed, magnetic flux, and power output to reproduce the dynamic characteristics found in a real wind turbine

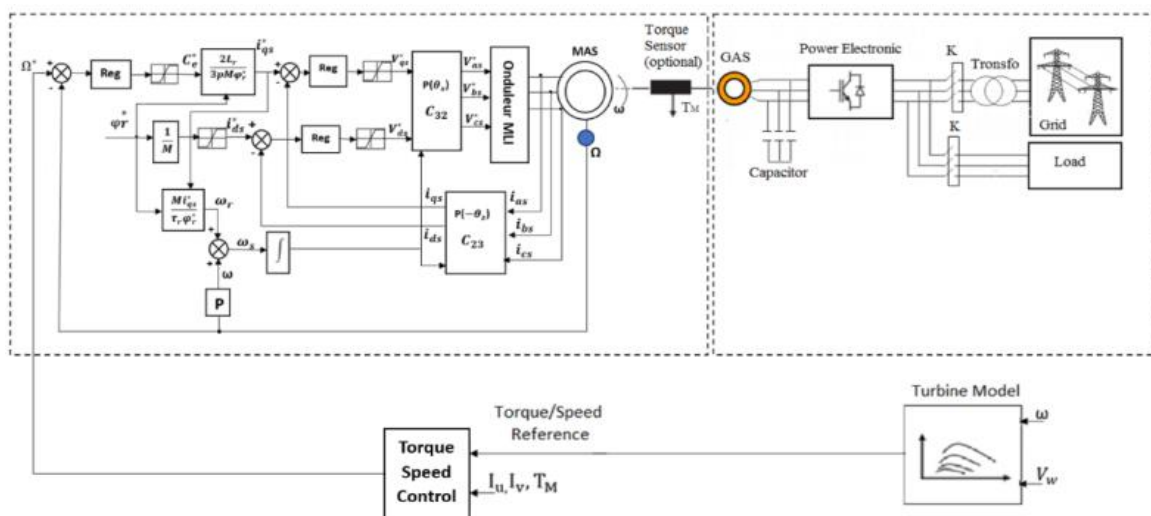


Figure 5. Configuration of the wind power emulator studied with the IRFOC command

3.2. Wind emulator design with DTC control integration

Figure 6 shows the detailed structure of the proposed wind emulator based on DTC, whose aim is to simulate the non-linear behavior of a real wind turbine. The structure is significantly simplified compared to vector control, since only one reference frame transformation is required, proportional and integral control loops have been replaced by hysteresis controllers, and no compensation decoupling is necessary. In general, our aim is to ensure good tracking of the reference stator flux from the reference current generated by the wind turbine mathematical model.

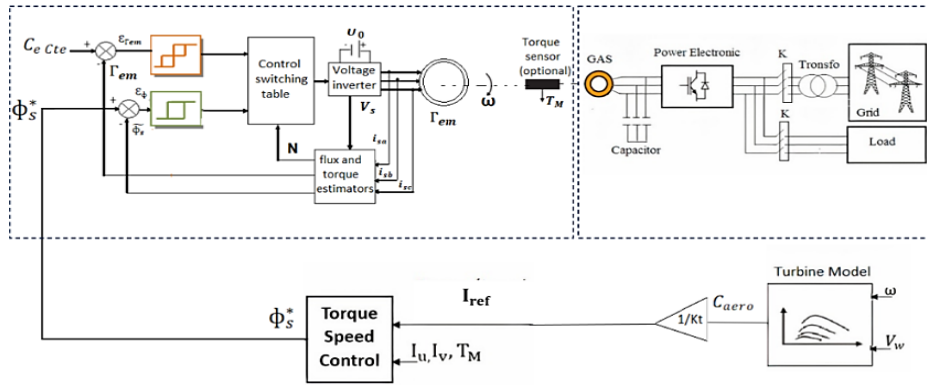


Figure 6. Configuration of the wind power emulator studied with DTC Control

4. RESULTS AND DISCUSSION

4.1. Simulation results IRFOC

This study examined the effects of wind turbine emulator control using an asynchronous motor, focusing specifically on DTC and IRFOC techniques. While previous studies have explored various aspects of wind turbine emulator control, they have not explicitly addressed the direct comparison between IRFOC and DTC techniques in this specific context. In this section, we propose to simulate and analyze the behavior of the wind emulator when wind speed varies abruptly, and to study its influence on the stability and performance of the emulator system by subjecting the system to a variable wind speed profile. A stepped wind profile was selected for this purpose. Figure 7 shows the first profile, which illustrates the evolution of wind speed in the MATLAB/Simulink environment (7 m/s – 9 m/s – 8 m/s).

Figure 8 shows the variation in shaft speed of the drive motor (main motor) and the turbine speed used as a reference speed. We can see that in the event of a sudden increase in wind speed (7 m/s to 9 m/s), the rotational speed of the drive motor shaft follows the rotational speed of the turbine with a delay of 1.2 seconds. However, during a sudden decrease in wind speed (9 m/s to 8 m/s), tracking is satisfactory, with a delay of around 0.1 second.

The Figure 9 shows the second profile illustrating the evolution of wind speed in the MATLAB/Simulink environment (5 m/s – 6 m/s – 9 m/s). Figure 10 illustrates the variation in rotational speed of the drive motor shaft (main motor) and the rotational speed of the turbine used as a reference. When the emulator is started up with a wind speed of 5 m/s, the response time for tracking the emulator speed and the turbine speed is around 0.6 s. Similarly, for a variation from 5 m/s to 6 m/s, the tracking time is of the order of 0.1 s. However, for a rapid increase from 6 m/s to 9 m/s, the error reaches a time value of 1.5 s. It can be seen that the time error increases significantly with a wide variation in wind speed.

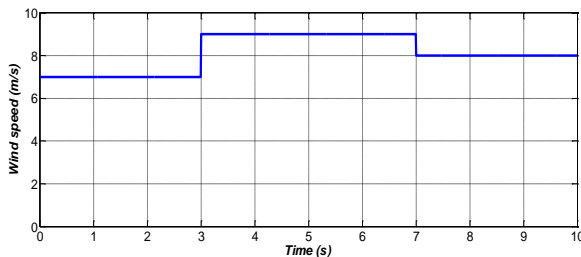


Figure 7. Wind speed profile (7 m/s – 9 m/s – 8 m/s)

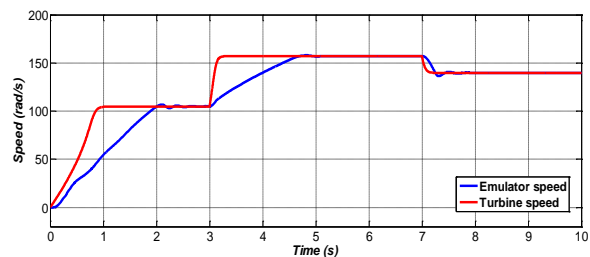


Figure 8. Variation in drive motor shaft speed (main motor) and turbine speed

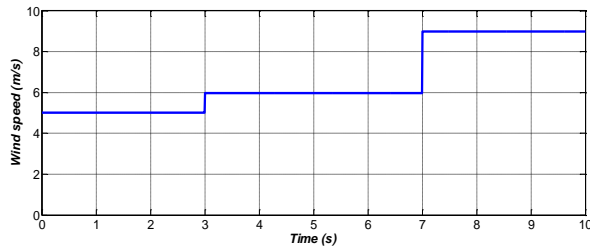


Figure 9. Wind speed sample (5 m/s – 6 m/s – 9 m/s)

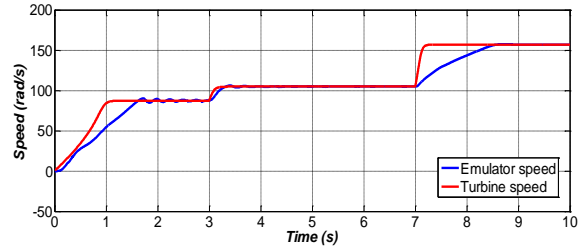


Figure 10. Variation of drive motor shaft speed (main motor) and turbine speed

Figure 11 shows the third wind profile, illustrating the evolution of wind speed in the MATLAB/Simulink environment (5 m/s – 7 m/s – 4 m/s). Figure 12 illustrates the variation in turbine rotation speed and emulator rotation speed during a sudden change in wind speed, from 5 m/s to 7 m/s, then from 7 m/s to 4 m/s. We observe that even with a significant decrease in wind speed (from 7 m/s to 4 m/s), the response time is of the order of zero. However, the error becomes high with a sudden increase in wind speed.

Figure 13 shows the variation in stator current with changing wind speed. Figure 13(a) illustrates this variation for a wind speed of 5 m/s, while Figure 13(b) shows it for a wind speed of 4 m/s. For a wind speed of 5 m/s, the current fluctuates from 5A to 12A. For a wind speed of 4 m/s, the current variation increases from 8A to 20A. We can see that the stator current is unstable in the event of a sudden change in wind speed.

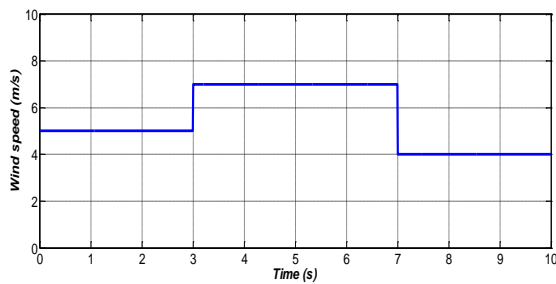


Figure 11. Wind speed samples (5 m/s – 7 m/s – 4 m/s)

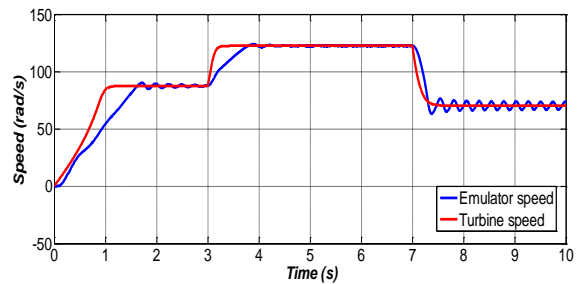
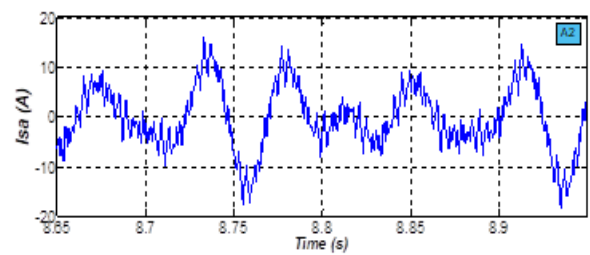
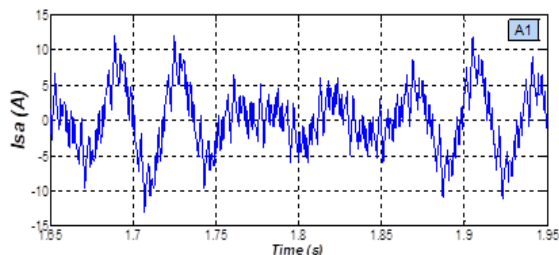
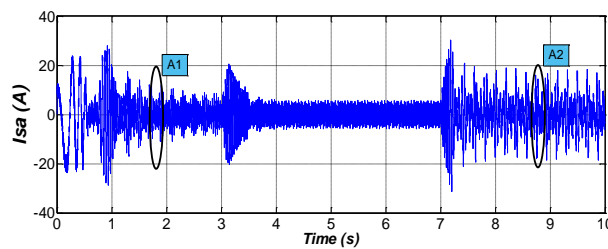


Figure 12. Variation of drive motor shaft speed (main motor) and turbine speed



(a)

(b)

Figure 13. Variation of stator current for a wind speed variation (a) 5 m/s and (b) 4 m/s

Figure 14 shows the variation in rotor current with changing wind speed. Figure 14(a) illustrates this variation for a wind speed of 5 m/s, while Figure 14(b) shows it for a wind speed of 4 m/s. For the variation in speed from 5 m/s to 4 m/s, we see current oscillations of the order of 5A, resulting in a remarkable instability of the rotor current.

The PWM voltage inverter provides a signal of variable frequency and amplitude. The waveform is obtained by comparing a 50 Hz signal with a sawtooth signal. The waveform obtained at the output is illustrated in the Figure 15. In Figure 15(a), we observe the output voltage waveform of the sinusoidal PWM-controlled inverter at a wind speed of 5 m/s. This figure illustrates the voltage waveform produced by the inverter at this specific wind speed. In Figure 15(b), we have the same output voltage waveform, but this time at a wind speed of 7 m/s. Compared with Figure 15(a), we can see variations in the voltage waveform due to the higher wind speed. Finally, in Figure 15(c), the output voltage waveform is shown for a wind speed of 4 m/s. Here, we can also observe variations in the voltage waveform, but this time due to a lower wind speed than in the other cases. In summary, these figures illustrate how the inverter output voltage waveform varies with wind speed, highlighting the impact of this variable on the power system.

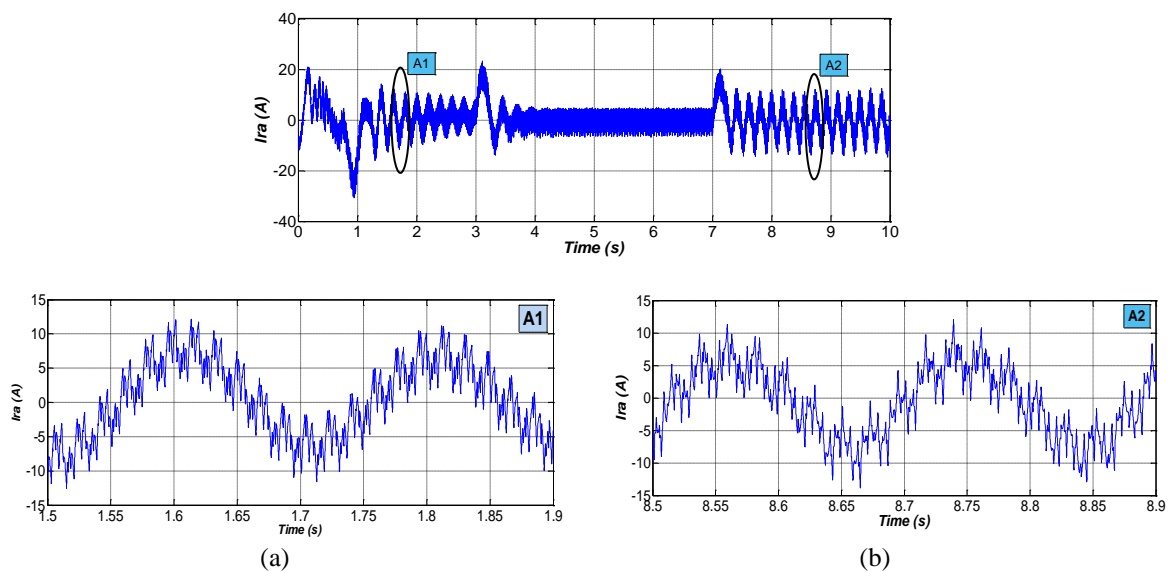


Figure 14. Variation of rotor current for a wind speed variation (a) 5 m/s and (b) 4 m/s

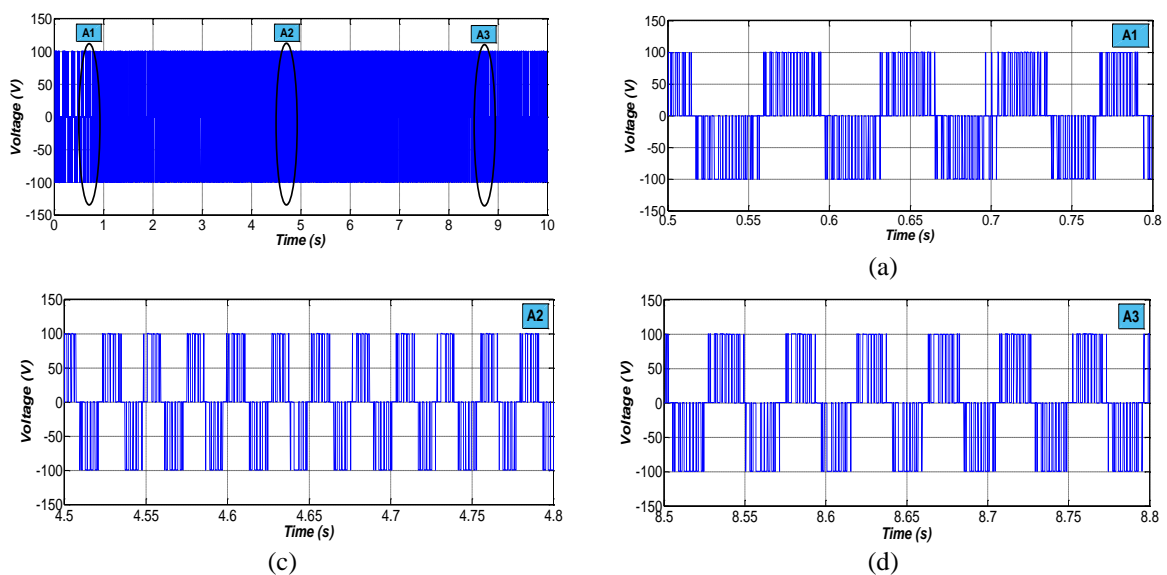


Figure 15. Inverter output voltage form controlled by PWM sine wave: (a) 5 m/s, (b) 7 m/s, and (c) 4 m/s

4.2. Simulation results DTC

The wind speed profile used in this section is illustrated in Figure 16. It is a pseudo-random signal constructed based on a series of steps (2 samples) ranging from 8 to 11 m/s. Even though real wind does not occur with such steep slopes, the series of steps proposed are standard signals that allow us to clearly interpret the system's behavior. Figure 17 shows the variation in rotational speed of the drive motor shaft. We can see that the speed of rotation of the shaft of the drive motor (main motor) follows the reference speed setpoint (wind speed) with a response time of the order of a few milliseconds.

Figure 18 represents the stator flux in the complex plane (α , β), starting from the point (0,0), and describing circular trajectories corresponding to the wind speed variation from 8m/s to 9m/s and then to 11 m/s. These trajectories follow circles with radii of 0.4 Wb for 8 m/s, 0.5 Wb for 9 m/s, and 0.7 Wb for 11 m/s. The wind speed profile used in this section is shown in Figure 19. For a second test, we chose a different speed profile from the one used in the first test. In order to guarantee the correct operation of our system, we used a pseudo-random signal constructed from a series of steps (2 samples) between 9 and 10 m/s.

Figure 20 shows the variation in rotational speed of the drive motor shaft. On close examination, we can see that the speed of rotation of this shaft precisely follows the reference speed setpoint (wind speed), with a response time of the order of a few milliseconds. Figure 21 shows the stator flux in the complex plane (α , β), starting from the point (0, 0), and describing circular trajectories corresponding to the variation in wind speed from 9 m/s to 7 m/s, then to 10 m/s. These trajectories follow circles of radius 0.5 Wb for 9 m/s, 0.3 Wb for 7 m/s, then 1Wb for 10 m/s.

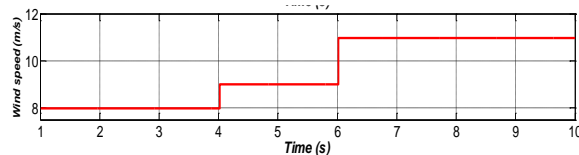


Figure 16. Wind speed samples (8 m/s, 9 m/s, 11 m/s)

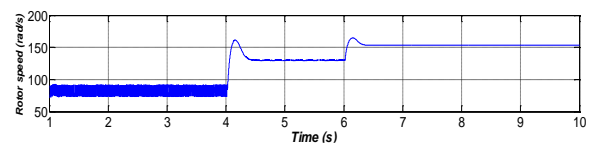


Figure 17. Variation of drive motor shaft speed (Main motor)

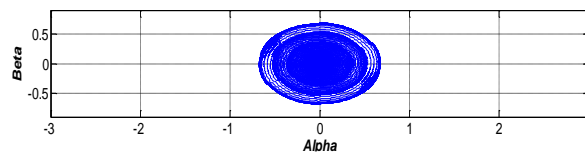


Figure 18. Stator flux trajectory on the α and β planes

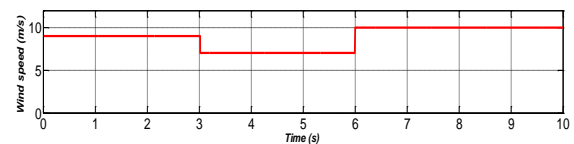


Figure 19. Wind speed profile (9 m/s, 7 m/s, 10 m/s)

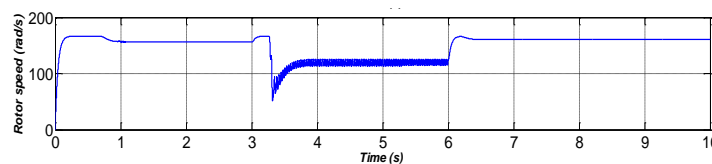


Figure 20. Variation in the rotation speed of the drive shaft of the drive motor

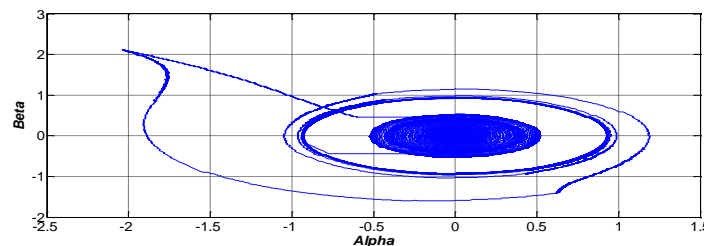


Figure 21. Stator flux trajectory on the α and β planes

Figure 22 illustrates the variation of stator current in the α plane as a function of wind speed. In Figure 22(a), we observe this variation for a wind speed of 9 m/s. This curve illustrates how the stator current evolves in response to wind speed fluctuations in this specific speed. On the other hand, in Figure 22(b), we have the same variation in stator current in the α plane, but this time for a wind speed of 10 m/s. Comparing the two figures, we can see the differences in stator current profiles at different wind speeds. These variations highlight the impact of wind speed on the stator current of the power system.

Figure 23 shows the variation of stator current in the β plane as a function of wind speed. Figure 23(a) shows this variation for a wind speed of 9 m/s, while Figure 23(b) represents it for a wind speed of 10 m/s. These graphs highlight the changes in stator current during a variation in wind speed, specifically observed in the β plane.

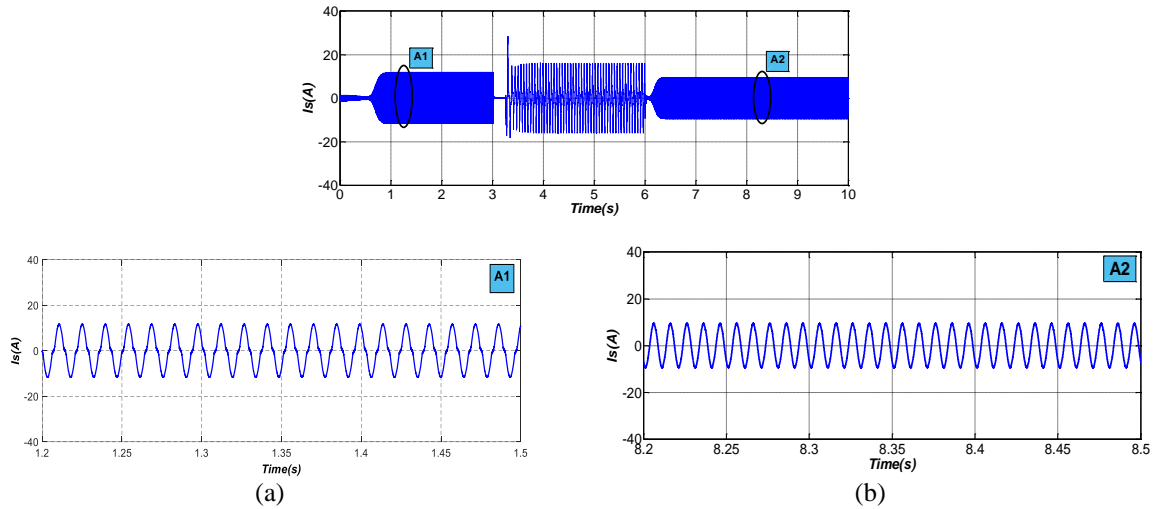


Figure 22. Stator current variation in the alpha plane for a variation in wind speed (a) 9m/s and (b) 10m/s

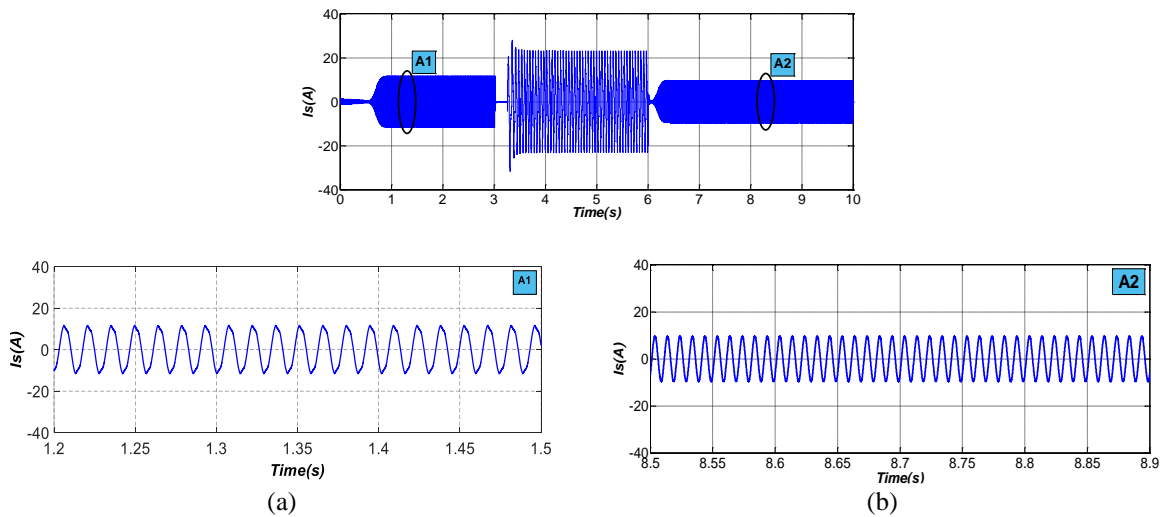


Figure 23. Stator current variation in the Beta plane for a variation in wind speed (a) 9 m/s and (b) 10 m/s

It can be seen that at wind speeds of 9 m and 10 m/s, the stator current along the Alpha axis is around 10 A and 9.5 A respectively. It is also observed that the current oscillations obtained in the case of DTC control are significantly lower than in the case of IRFOC control. Comparing our results with other studies, notably that of [23] on flux vector control and direct torque control of the asynchronous machine, our conclusion is in line with the trend observed in the literature. We found that DTC control exhibits a faster response time during sudden variations in wind speed, as well as a noticeable reduction in stator and rotor

current oscillations compared to IRFOC control. Although both methods demonstrated good setpoint tracking, these observations suggest that the DTC method can improve the responsiveness and reduce the mechanical vibrations of wind turbine emulators, without compromising other performances.

In Figure 24, we examine the voltage waveform produced at the output of the inverter, controlled by sinusoidal PWM. In Figure 24(a), the voltage waveform is observed for a wind speed of 9 m/s, illustrating the voltage fluctuations specific to this speed. Figure 24(b) presents the waveform for a wind speed of 7 m/s, showing slightly different fluctuations from the first. Finally, in Figure 24(c), the waveform is shown for a wind speed of 10 m/s, with distinct fluctuations corresponding to this speed.

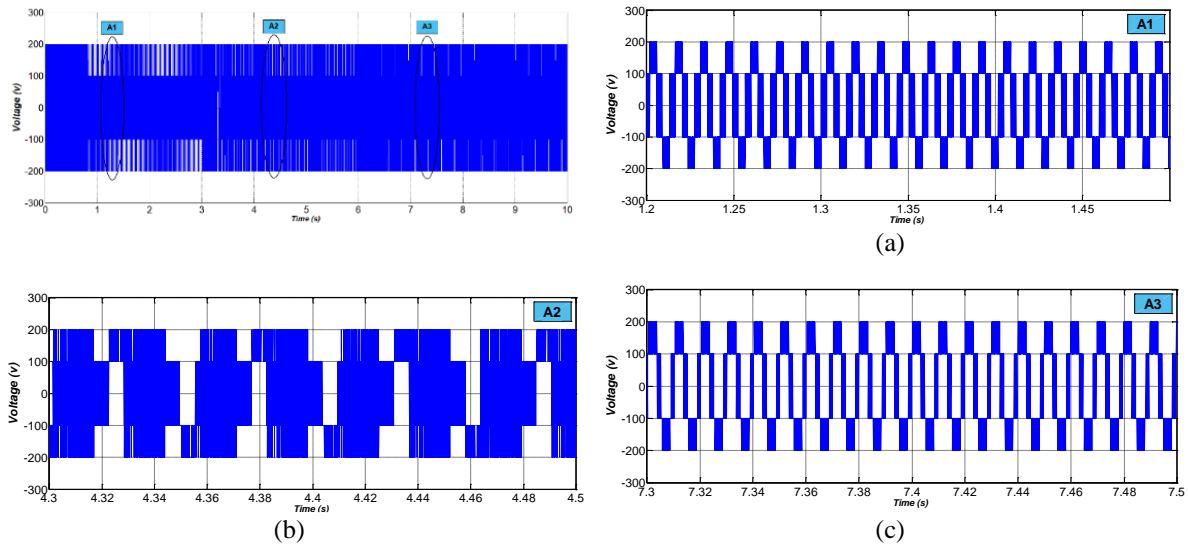


Figure 24. Inverter output voltage shape controlled by PWM Sine wave: (a) 9 m/s, (b) 7 m/s, and (c) 10 m/s

This study examined in depth the effects of IRFOC and DTC methods on the control of wind turbine emulators using an asynchronous motor. Our results indicate that DTC control offers better responsiveness and reduces mechanical vibrations compared to IRFOC. However, further studies are needed to confirm these results under various operational conditions and further explore the potential of DTC. Future research could also compare DTC with other emerging techniques to better assess its advantages and limitations, thus contributing to the optimization of wind turbine emulators for better integration into power grids.

5. RESULTS INTERPRETATION

The results show the performance of the two methods studied IRFOC and DTC with some differences. They also show good setpoint tracking for both study cases. During a sudden increase in wind speed, which generates a mechanical speed on the wind turbine shaft (reference signal) based on the turbine model proposed in MATLAB/Simulink, we note that the response time between this reference signal and the signal generated on the asynchronous generator shaft is lower (a few ms) in the case of DTC control. It's also worth noting that the stator and rotor current oscillations obtained with the DTC control (sinusoidal form) are lower than those of the IRFOC control, hence the minimization of mechanical vibrations on the wind turbine shaft (less heating, which implies fewer joule losses). With a view to the future, we have opted to implement both controllers in real time on a Dspace DS1104 board. We're also looking into other methods and configurations.

6. CONCLUSION

This article presents an analytical and comparative study of IRFOC and DTC applied to an asynchronous machine. This analysis is part of the design and implementation of a variable-speed wind emulator based on the asynchronous machine. First, we modeled the wind emulator (model of the wind turbine and the asynchronous machine) with the two closed-loop control programs IRFOC and DTC in MATLAB/Simulink. Secondly, we analyzed the simulation results to make comparative studies and validate the appropriate emulator model. The aim was to understand performance in the field of wind emulation. The results highlighted the strengths and limitations of each technique to guide the choice of control

strategies in emulated wind systems. Finally, in the perspective of future developments, it would be relevant to explore collaboration between these approaches and improve the design of wind emulators to contribute to the evolution of wind energy conversion technologies and the integration of this proposed model into an intelligent computing board.

REFERENCES

- [1] T. Ouchbel *et al.*, “Power maximization of an asynchronous wind turbine with a variable speed feeding a centrifugal pump,” *Energy Conversion and Management*, vol. 78, pp. 976–984, Feb. 2014, doi: 10.1016/j.enconman.2013.08.063.
- [2] T. Ouchbel, S. Zouggar, M. L. Elhafyani, M. Mokhtari, M. Oukili, and F. Zahra Kadda, “Control of a variable speed asynchronous wind turbine dedicated to isolated site,” *Indonesian Journal of Electrical Engineering and Computer Science*, vol. 20, no. 2, p. 627, Nov. 2020, doi: 10.11591/ijeecs.v20.i2.pp627-637.
- [3] T. Ouchbel, S. Zouggar, M. Sedik, M. Oukili, M. Elhafyani, and A. Rabhi, “Control of the output voltage of asynchronous wind turbine with variable speed using a static VAR compensator (SVC),” in *Smart Innovation, Systems and Technologies*, vol. 12, 2012, pp. 17–30.
- [4] T. Ouchbel, S. Zouggar, M. L. Elhafyani, M. Oukili, M. Sedik, and A. Rabhi, “Regulation of the excitation reactive power of the asynchronous wind turbine at variable speed,” *Smart Grid and Renewable Energy*, vol. 04, no. 03, pp. 272–280, 2013, doi: 10.4236/sgre.2013.43033.
- [5] M. Mokhtari, S. Zouggar, M. L. Elhafyani, T. Ouchbel, S. Benzaouia, and M. Fannakh, “Design, simulation and performance analysis of voltage regulator based on STATCOM for asynchronous wind turbine,” in *Lecture Notes in Electrical Engineering*, vol. 519, 2019, pp. 498–509.
- [6] M. Mokhtari, S. Zouggar, M. L. Elhafyani, T. Ouchbel, N. K. M’Sirdi, and A. Naaman, “Voltage stability improvement of an asynchronous wind turbine using static var compensator with single input fuzzy logic controller,” in *2018 6th International Renewable and Sustainable Energy Conference (IRSEC)*, Dec. 2018, pp. 1–6, doi: 10.1109/IRSEC.2018.8702872.
- [7] O. Benzohra, S. S. Echcharqaouy, F. Fraija, and D. Saifaoui, “Integrating wind energy into the power grid: impact and solutions,” *Materials Today: Proceedings*, vol. 30, pp. 987–992, 2020, doi: 10.1016/j.matpr.2020.04.363.
- [8] S. Zouggar, Y. Zidani, M. L. Elhafyani, T. Ouchbel, M. Seddik, and M. Oukili, “Neural control of the self-excited induction generator for variable-speed wind turbine generation,” in *Smart Innovation, Systems and Technologies*, vol. 12, 2012, pp. 213–223.
- [9] S. Benzaouia, M. Mokhtari, S. Zouggar, A. Rabhi, M. L. Elhafyani, and T. Ouchbel, “Design and implementation details of a low cost sensorless emulator for variable speed wind turbines,” *Sustainable Energy, Grids and Networks*, vol. 26, p. 100431, Jun. 2021, doi: 10.1016/j.segan.2021.100431.
- [10] R. S. Hiware and J. G. Chaudhari, “Indirect field oriented control for induction motor,” in *International Conference on Emerging Trends in Engineering and Technology, ICETET*, Nov. 2011, pp. 191–194, doi: 10.1109/ICETET.2011.56.
- [11] D. Casadei, G. Serra, A. Tani, and L. Zarri, “Direct torque control for induction machines: a technology status review,” in *Proceedings - 2013 IEEE Workshop on Electrical Machines Design, Control and Diagnosis, WEMDCD 2013*, Mar. 2013, pp. 117–129, doi: 10.1109/WEMDCD.2013.6525172.
- [12] F. Niu, B. Wang, A. S. Babel, K. Li, and E. G. Strangas, “Comparative evaluation of direct torque control strategies for permanent magnet synchronous machines,” *IEEE Transactions on Power Electronics*, vol. 31, no. 2, pp. 1408–1424, Feb. 2016, doi: 10.1109/TPEL.2015.2421321.
- [13] A. Sajadi, Ł. Rosłaniec, M. Kłos, P. Biczal, and K. A. Loparo, “An emulator for fixed pitch wind turbine studies,” *Renewable Energy*, vol. 87, pp. 391–402, Mar. 2016, doi: 10.1016/j.renene.2015.10.033.
- [14] J. Castelló, J. M. Espí, and R. García-Gil, “Development details and performance assessment of a wind turbine emulator,” *Renewable Energy*, vol. 86, pp. 848–857, Feb. 2016, doi: 10.1016/j.renene.2015.09.010.
- [15] F. Martinez, L. C. Herrero, and S. de Pablo, “Open loop wind turbine emulator,” *Renewable Energy*, vol. 63, pp. 212–221, Mar. 2014, doi: 10.1016/j.renene.2013.09.019.
- [16] M. A. Bhayo, M. J. A. Aziz, N. R. N. Idris, and A. H. M. Yatim, “Design and development of a wind turbine emulator for analyzing the performance of stand-alone wind energy conversion system,” *International Journal of Power Electronics and Drive Systems*, vol. 8, no. 1, pp. 454–461, 2017, doi: 10.11591/ijpeds.v8i1.pp454-461.
- [17] J. Yan, Y. Feng, and J. Dong, “Study on dynamic characteristic of wind turbine emulator based on PMSM,” *Renewable Energy*, vol. 97, pp. 731–736, Nov. 2016, doi: 10.1016/j.renene.2016.06.034.
- [18] P. S. Kumar, R. P. S. Chandrasena, and K. V. S. M. Babu, “Design and implementation of wind turbine emulator using FPGA for stand-alone applications,” *International Journal of Ambient Energy*, vol. 43, no. 1, pp. 2397–2409, Dec. 2022, doi: 10.1080/01430750.2020.1736152.
- [19] P. K. Behera, B. Mendi, S. K. Sarangi, and M. Pattnaik, “Robust wind turbine emulator design using sliding mode controller,” *Renewable Energy Focus*, vol. 36, pp. 79–88, Mar. 2021, doi: 10.1016/j.ref.2020.12.004.
- [20] S. Tammaruckwattana and K. Ohyama, “Experimental verification of variable speed wind power generation system using permanent magnet synchronous generator by wind turbine emulator,” in *IECON 2012 - 38th Annual Conference on IEEE Industrial Electronics Society*, Oct. 2012, pp. 5827–5832, doi: 10.1109/IECON.2012.6389131.
- [21] A. K. Yadav, M. Singh, and D. C. Meena, “Modelling and simulation of wind turbine emulator using DC motor,” in *2016 IEEE 7th Power India International Conference (PIICON)*, Nov. 2016, pp. 1–5, doi: 10.1109/POWERI.2016.8077317.
- [22] M. Aktas, K. Awaili, M. Ehsani, and A. Arisoy, “Direct torque control versus indirect field-oriented control of induction motors for electric vehicle applications,” *Engineering Science and Technology, an International Journal*, vol. 23, no. 5, pp. 1134–1143, Oct. 2020, doi: 10.1016/j.jestch.2020.04.002.
- [23] D. Du, C. D. E. La, and M. Asynchrone, “Etude comparative entre la commande vectorielle a flux oriente et la commande directe du couple de la machine asynchrone,” *Sci. Bull., Series*, vol. 69, no. 2, 2007.
- [24] Y. Wang, S. Đukanović, N. Sarma, and S. Djurović, “Implementation and performance evaluation of controller signal embedded sensorless speed estimation for wind turbine doubly fed induction generators,” *International Journal of Electrical Power and Energy Systems*, vol. 148, p. 108968, Jun. 2023, doi: 10.1016/j.ijepes.2023.108968.
- [25] M. E. Abdallah, O. M. Arafa, A. Shaltot, and G. A. A. Aziz, “Wind turbine emulation using permanent magnet synchronous motor,” *Journal of Electrical Systems and Information Technology*, vol. 5, no. 2, pp. 121–134, Sep. 2018, doi: 10.1016/j.jesit.2018.03.005.

BIOGRAPHIES OF AUTHORS

Hana Zekraoui    she obtained her University Diploma of Technology in Electrical Engineering and Renewable Energies from the Higher School of Technology of Oujda, Morocco, followed by a professional license degree in Electrical Engineering from the same institution. She then continued her studies by earning a master's degree in Electronics, Electrical Energy, and Automation at the University of Rennes 1, France. Currently, she is pursuing her Ph.D. in Physics and Engineering at the Faculty of Sciences, within the Electrical Engineering and Maintenance Laboratory of the Higher School of Technology Oujda, Morocco. She is a member of the multisource energy systems management team within the same laboratory. Her research topic focuses on the design and realization of a wind emulator based on a variable-speed asynchronous machine. This research reflects her ongoing commitment to the field of renewable energy and electrical engineering. She can be contacted at email: hanae.zekraoui@ump.ac.ma.



Taoufik Ouchbel    he received a Master of electronics and system of the communication from Faculty of Science Mohamed I University in 2008. In 2015 he received a Ph.D. degree in Power Electronics, from Faculty of Science, Mohamed I University. His research in renewable energy: wind power and photovoltaic systems. He is currently a full Professor of Electrical Engineering at Higher Institute of Technology, Mohamed I University, Oujda, Morocco, Member in Laboratory of Electrical Engineering and Maintenance at Higher Institute of Technology. He can be contacted at email: t.ouchbel@ump.ac.ma.



Mohamed Larbi El Hafyani    University Professor at Mohamed first university, Oujda, Morocco is currently member at Laboratory of Electrical Engineering and Maintenance (LEEM). He received the Diploma of higher studies advancedl in science from faculty of science, university Mohamed first, Oujda in 2003, He received with Honors the Ph.D. degree in electrical machines and power electronic (renewable energy), from faculty of science, university Mohamed first, Oujda in 2008. Since 2009 he has been a professor of power electronic and electrical machines. His current area of interest is related to the advanced control of wind turbine system, power electric, and renewable energy. He can be contacted at email: m.elhafyani@ump.ac.ma.